Article

Magnetic Nanofluid Droplet Impact on an AAO Surface with a Magnetic Field

Yu-Chin Chien [ID] **and Huei Chu Weng** * [ID]

Department of Mechanical Engineering, Chung Yuan Christian University, Taoyuan 32023, Taiwan; vance1829@gmail.com

* Correspondence: hcweng@cycu.edu.tw; Tel.: +886-3-265-4311

check for updates

Abstract: This paper presents an experimental study on the impact of magnetic nanofluid droplets on aluminum sheet surfaces subjected to a magnetic field. A magnetic nanofluid was prepared by synthesizing Fe_3O_4 nanoparticles and coating amounts of oleic acid surfactant in deionized water. The wettability of an alumina sheet was first changed by using a phosphoric acid (H_3PO_4) solution to perform the first anodic oxidation process. A contact angle meter and a high-speed camera were then, respectively, used to capture the static contact angle of magnetic nanofluid droplets and their dynamic characteristics during impact on the surface with/without anodic oxidation process. The results of the static contact angle showed that a more hydrophilic surface could be obtained after the sheet was processed. The dynamic images showed that the processed surface exhibited a slightly greater degree of adhesion between the liquid and solid without a magnetic field. The effect of AAO surface topography can be significant under the action of an external magnetic field.

1. Introduction

The dynamic behavior of droplets impacting solid surfaces has always been an attractive issue in interface impact studies due to its wide range of applications. In general, the dynamic behavior can be divided into several kinds of types, such as deposition, sticky vibrating, prompt splash, corona splash, receding break-up, partial rebound, and complete rebound [1,2]. Many studies have shown interest in various parameters, such as contact time, bouncing off surface, bouncing height, rebound number, deposition, and spreading diameter. Different parameters of the impact droplet dominate the corresponding application areas. For example, the effect of a shorter contact time or bouncing off surface is an important consideration in anti-icing [3] and self-cleaning [4] applications, which are able to prevent water or dust from adhering to surfaces. On the contrary, in spray cooling [5], a longer contact time or deposition can keep the water on the surface and further enhance the heat removal efficiency. In order to reduce the amount of materials used in spray coating and painting [6], the maximum spreading diameter is a parameter of interest. It is also particularly important in other applications, like plasma spraying [7], pharmaceutical industry [8], ink-jet printing [9], metal forming [10,11], and combustion [12,13].

In 1876, Worthington was first drawn to an interesting phenomenon of milk or mercury droplet impact on a smoked glass plate, showing the complex shapes [14]. It was revealed that the droplet separation and elongation increases when the height of the fall is increased. In general, when a droplet is impacting on a solid surface, the deformation of the droplet is affected by the properties of the liquid (impact velocity, size, density, surface tension, viscosity, etc.) and solid surface (morphology, roughness, adhesion force, etc.). Some parameters are usually expressed by two dimensionless numbers, the Weber

number (We) and the Reynolds number (Re). Here, We $= \rho V_0^2 d_0 / \sigma$ characterizes the ratio of kinetic energy to the surface energy and Re $= \rho V_0 d_0 / \mu$ describes the ratio of inertial forces to viscous forces, where ρ is the density of liquid droplets; V_0 and d_0 are the droplet initial impact velocity and diameter, respectively; σ is the surface tension of liquid droplets; and μ is the viscosity of liquid droplets. Zhang et al. [15] reported an experimental study on the impact force of different droplets colliding with a flat polished aluminum plate. The dimensionless impact force is independent of the Weber number in the range of 68 < We < 858, but changes with the Reynolds number. The change in surface tension has little effect on peak force in the range of 68 < We < 858. In the viscosity-dominated zone (2.9 < Re < 20), the effect of viscosity plays an important role in dimensionless impact force. Yonemoto and Kunugi [16] developed an analytical model for predicting the dimensionless maximum spreading diameter (the maximum spreading diameter normalized in terms of initial droplet diameter).

On the other hand, some studies have focused on examining the droplet impact under different surface conditions. An experimental study on the spreading of water droplets impinging on the rough surface was conducted by Sivakumar et al. [17]. The texture pattern of the substrate may make the spreading pattern of an impacting droplet spread asymmetrically and further lead the liquid to splash. Liu et al. [18] showed that the pillared surfaces with a larger apex angle could induce larger robust pancake bouncing. Patil et al. [19] introduced the impact dynamics of a microliter water droplet on a micropillared hydrophobic surface with different pitch of the pillars. Increased spacing of pillars will result in different bouncing regimes (from non-bouncing to complete bouncing, to partial bouncing, then back to non-bouncing). Malla et al. [20] used photolithography to fabricate a hydrophobic microgrooved surface. It was reported that the phenomenon of droplet bouncing with breakup is dependent on the pitch of the grooved surface and the Weber number. Shen et al. [21] showed that convex superhydrophobic surfaces could result in a 28.5% reduction in droplet-surface contact time compared with flat superhydrophobic surfaces. In fact, the effect of nanostructure on the droplet impact on the surface is also investigated in some studies [22]. Tsai et al. [23] introduced water droplet impact dynamics onto micro- and nanostructured superhydrophobic surfaces. The results indicated that the nanoscale on multiscale surface roughness plays an important role in the impact process for higher Weber numbers (We $\geq$ 120). Raza et al. [24] investigated the dynamic behavior of microliter droplets impacting on hydrophobic surfaces with hierarchical roughness. The number of droplet bouncing events was exponentially increased by increasing the hydrophobicity of the surface, which was coated with gold nanoparticles. Liu et al. [3] fabricated a micro/nanostructure on aluminum alloy surfaces. The experiment displayed an excellent anti-icing property and droplet rebounding activity.

Recently, a suspension of nanoparticles in a base fluid, the so-called nanofluid, has been used in a number of studies due to the unique thermal-fluid properties [25], like spray cooling [26,27], solar collector [28], and engine oil [29]. In droplet impingement studies, Murshed and de Castro [30] reported that the spreading characteristics of TiO_2/ethylene glycol nanofluid droplet impinged on aluminum surfaces. It was seen that the spreading diameter increases as the volume fraction of nanoparticles also increases. Kahani et al. [31] experimentally observed the dynamic and heat transfer performances of TiO_2/water nanofluid droplet impact on a silicon surface with no coating, a superhydrophobic coating, and a superhydrophilic coating. It has shown that the cooling effectiveness could be enhanced by dispersing TiO_2 nanoparticles in water droplets. However, the superhydrophobicity results in a reduction in cooling energy due to the smaller wetted area and the shorter contact time. Compared to conventional nanofluids, magnetic nanofluids possess magnetically controllable properties under magnetic fields [32–34]. In order to accurately control the magnetic nanofluids in fluidic devices and energy systems, it is very important to understand the static and dynamic magnetowetting [35]. The shape and contact angle of a magnetic nanofluid sessile droplet in magnetic fields were investigated experimentally and numerically in some recent studies. Nguyen et al. [36] observed the magnetowetting of a sessile magnetic nanofluid droplet on a planar surface. The experimental results showed that the shape of the sessile droplet is flattened and the contact angle is reduced as the magnetic flux increases. Manukyan and Schneider [37] further

investigated the magnetowetting of an oil-based magnetic nanofluid and a water-based magnetic paint on a hydrophobic flat surface. The elongated shape of a magnetic nanofluid droplet and the flattened shape of a magnetic paint droplet were observed under an external magnetic field. In the experiment, it was observed that as the magnetic field increases from 0 to 20 mT, the magnetic nanofluid droplet contact angle decreases first and then increases; however, as the magnetic field increases from 100 to 300 mT, the magnetic paint droplet contact angle increases first and then decreases. Rigoni et al. [38] investigated the effects of a magnetic field and nanoparticle concentration on the magnetowetting of water-based magnetic nanofluids. They found that the shape of a magnetic nanofluid droplet can be changed by applying a magnetic field gradient. The above magnetic field effect can be further enhanced by increasing the nanoparticle concentration. Chien and Weng [39] numerically studied the profile change of magnetic nanofluid sessile droplets under an applied magnetic field gradient by using a revision of the classic Young–Laplace equation according to normal stress balance principles. The results showed that a downward magnetic force can be used to flatten the droplets and reduce the contact angle, while an upward magnetic force can be used to elongate the droplets and increase the contact angle. The influence of surface morphology on the magnetowetting of magnetic nanofluids was further investigated by Chien and Weng [40]. It was found that the magnetic field generally has a more significant magnetowetting effect on smaller-AAO-pore-size surfaces.

As mentioned above, the static magnetowetting of magnetic nanofluids on a surface has been investigated. However, the dynamic behavior of magnetic nanofluid droplets on a surface under the action of an external magnetic field has not been studied. Therefore, this study experimentally investigated the effect of surface morphology on the dynamic characteristics of the magnetic nanofluid droplet impact on an alumina surface with/without an anodic oxidation process in an applied magnetic field by using a high-speed camera.

2. Materials and Methods

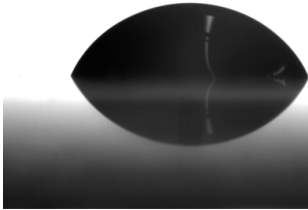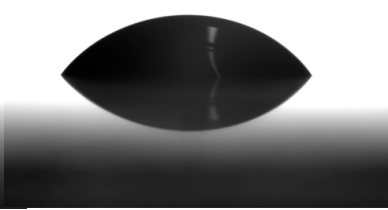### 2.1. Preparation of Magnetic Nanofluids

The magnetite (Fe_3O_4) nanoparticles were synthesized according to the co-precipitation method [41,42]. In brief, a mixture of ferrous chloride tetrahydrate ($FeCl_2 \cdot 4H_2O$) and ferric chloride anhydrous ($FeCl_3$) acid solution (100 mL, molarity: $Fe^{2+}/Fe^{3+} = 1/2$) was added to a sodium hydroxide (NaOH) alkaline solution (50 mL, 8 M) to obtain Fe_3O_4 nanoparticles after the solution was cooled down to room temperature (25 °C). Then, these nanoparticles were washed by deionized water to remove the salt impurities several times. Next, the NaOH alkaline solution (12 M) was mixed with Fe_3O_4 nanoparticles to obtain the 200 mL unstable water-based magnetite nanofluids. Because the Fe_3O_4 nanoparticles may aggregate and precipitate under the action of a gravitational or magnetic force, 5 mL oleic acid ($C_{18}H_{34}O_2$) was used to cover Fe_3O_4 nanoparticles. The changes in fluid electrical conductivity over time have been used to estimate the stability of magnetic nanofluids [43]. From the obtained conductivity-time relationship, the electrical conductivity decreased by a maximum of 18.41% in one hour. To avoid the influence of fluid instability, all experimental measurement processes were set to be completed within 20 min. Finally, the volume fraction of particles of the stable water-based Fe_3O_4 nanofluids used in this work was estimated to be 1.00%.

2.2. Preparation of Aluminum Sheet Surfaces

In order to obtain two different wettability types of surface, an anodic oxidation process was adopted. An aluminum sheet (purity: 99.5%; 50 × 50 × 0.2 mm) was first cleaned in acetone (C_3H_6O), ethanol (C_2H_5OH), and deionized water by an ultrasonic cleaner for 5 min. Then, the randomly formed anodic aluminum oxide (AAO) structure was performed by the first anodic oxidation process while applying 20 V in 0.3 M phosphoric acid (H_3PO_4) solution at 5 °C for 180 min. The surface wettability was assessed by measuring the contact angle of a magnetic nanofluid sessile droplet (~6 μL) using a contact angle meter through the conic method (Model 100SL with an accuracy of 0.01°, Sindatek) at

room temperature. The value of each contact angle is the average value obtained by five independent measurements with absolute relative uncertainty of less than 10.98%. As shown in Table 1, the static contact angle of magnetic nanofluids decreased from $66.12 \pm 1.68°$ to $53.01 \pm 5.82°$ after the aluminum sheet was processed at a particular anodizing voltage (20 V). The decrease in the contact angle on the processed surface is attributed to the presence of nanostructures. The nanostructures may lead to the enhancement of the capillary force on the solid surface. As a result, more surface will be wetted by the droplets and thus the area covered will increase. It should be noted that before the experiment in this study, all aluminum sheets had been immersed in ethanol at 25 °C for 180 min to break the hydrogen bonds and baked using a vacuum oven at 100 °C for 60 min, and their surface free energies have been calculated by using the contact angles of two test liquids (deionized water and glycerol) through the Owens-Wendt-Rabel-Kaelble (OWRK) method. The calculated surface free energy is 153.94 mN/m (polar part: 133.96 mN/m; dispersive part: 19.99 mN/m) for the processed surface and 53.48 mN/m (polar part: 52.07 mN/m; dispersive part: 1.41 mN/m) for the unprocessed surface.

Table 1. Static magnetic nanofluid sessile droplet on aluminum surfaces.

Process	without anodic oxidation	with anodic oxidation
Appearance		
Contact angle	$66.12 \pm 1.68°$	$53.01 \pm 5.82°$

2.3. Experimental Steup

The schematic diagram of the experimental setup is shown in Figure 1. The droplets had a constant volume (~0.02 mL), generated by a peristaltic pump and then free fall at the tip of a dispensing needle. The falling distance was set at 150 mm. To generate a magnetic force, a neodymium magnet was used to produce magnetic field gradients (from 0 to 72×10^5 A/m^2) at the solid surface position. The magnetic field gradient was determined by using a Tesla meter (Model TM-701 with an indication accuracy of (5% of measurement value + 0.05) mT, KANETEC, Bensenville, IL, USA). The dynamic impingement of the droplet was recorded using a PCO. dimas HS high speed camera with a 30° angle from the horizontal at a frame rate of 2000 fps; a Zeiss lens (makro-planar 50 mm f/2) was connected to the camera to focus the images. The camera was operated using the commercial software Camware on a laptop.
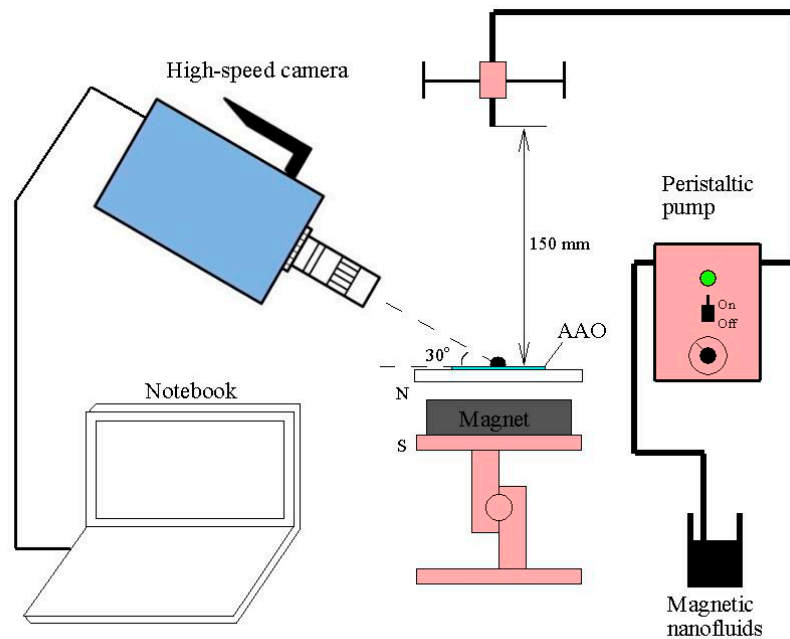
Figure 1. Schematic diagram of the experimental setup.

3. Results and Discussion

Now we will pay attention to the problem of the magnetic nanofluid droplet impact on an AAO surface with a magnetic field. The captured dynamic images are shown in Table 2 to investigate the effect of surface morphology on the dynamic magnetowetting of magnetic nanofluids on an alumina surface with/without an anodic oxidation process with/without the action of an external magnetic field. In addition, the reduced diameter D^*, defined as the ratio of the final wetted diameter and maximum extended diameter, is used to characterize the relative wetted size during the magnetic nanofluid droplet impact on a surface at different magnetic field gradients, as shown in Figure 2. Here, the diameter refers to the maximum length of the droplet-solid contact surface in the horizontal direction.

Table 2. Simultaneous high-speed images captured for the (**a**) unprocessed surface, (**b**) unprocessed surface with a magnetic field (72×10^5 A/m^2), (**c**) processed surface, and (**d**) processed surface with a magnetic field (72×10^5 A/m^2).
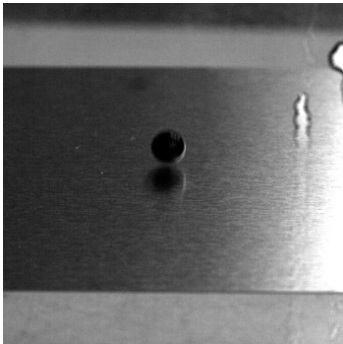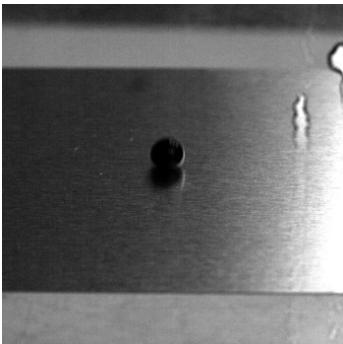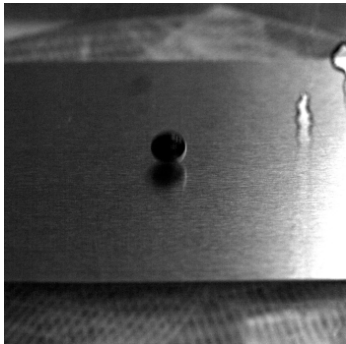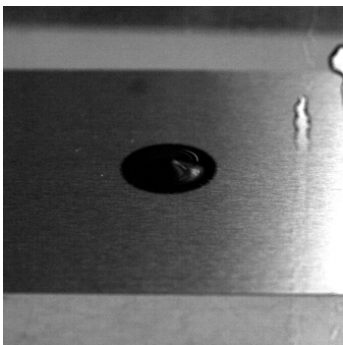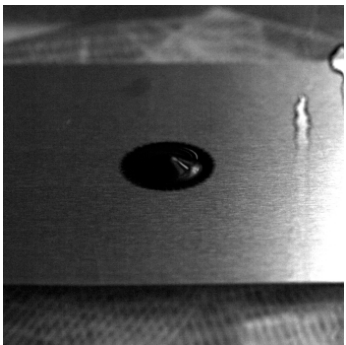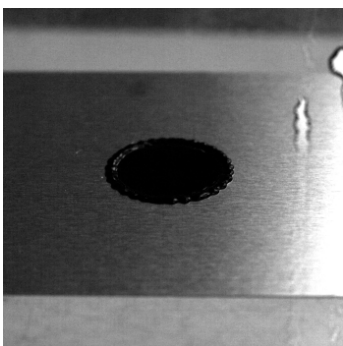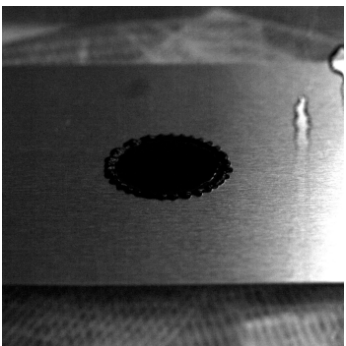
Time (ms)	(a)	(b)
−0.5		
0		
2		
6		

Table 2. *Cont.*
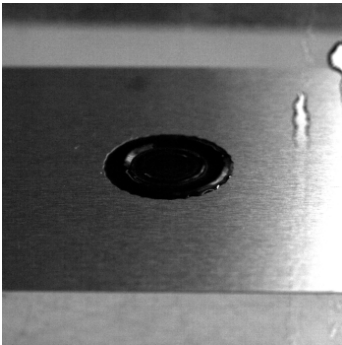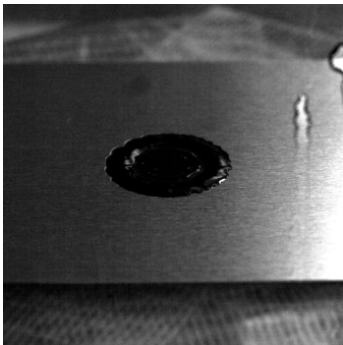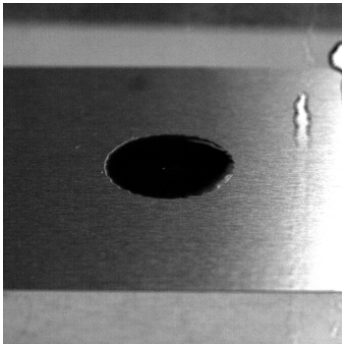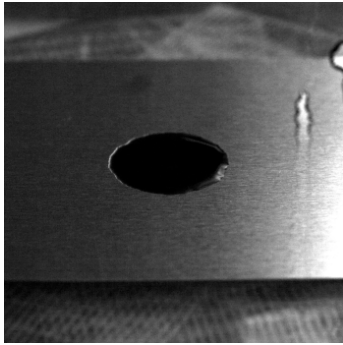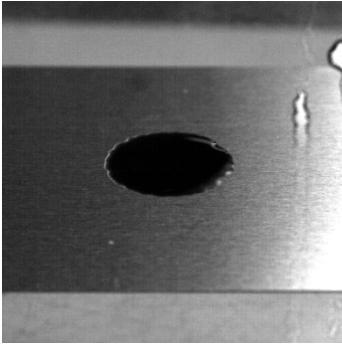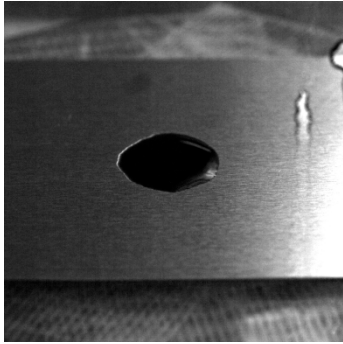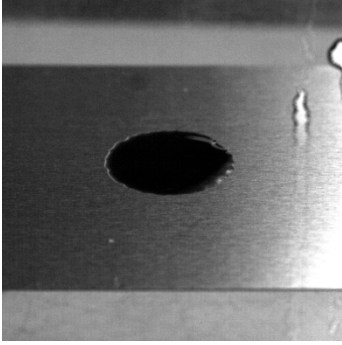
Time (ms)	(a)	(b)
14		
30		
100		
200		

Table 2. *Cont.*
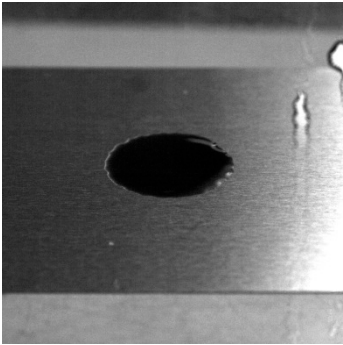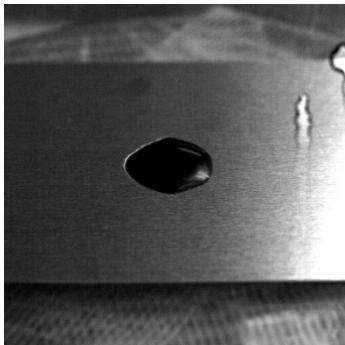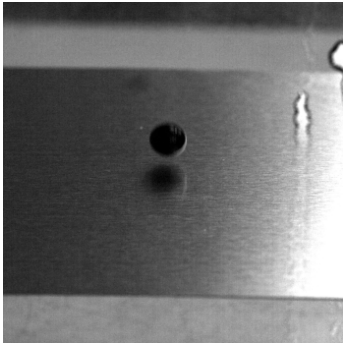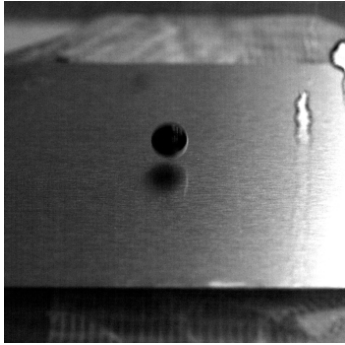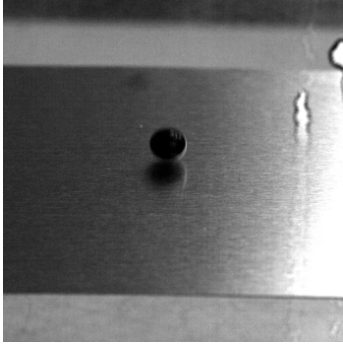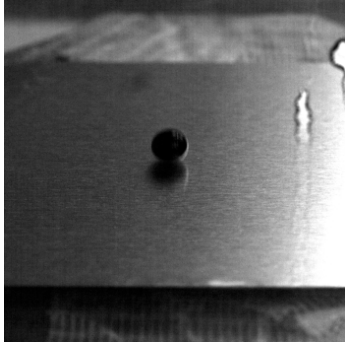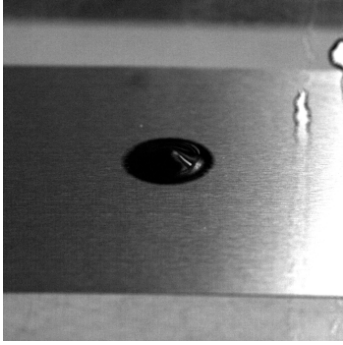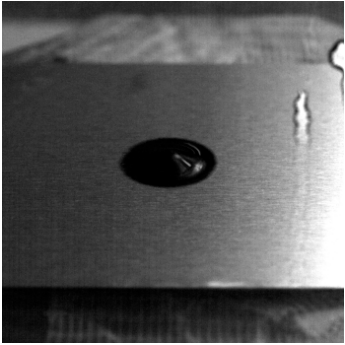
Time (ms)	(a)	(b)
300		
−0.5		
0		
2		

Table 2. *Cont.*
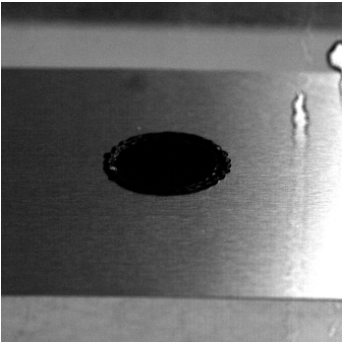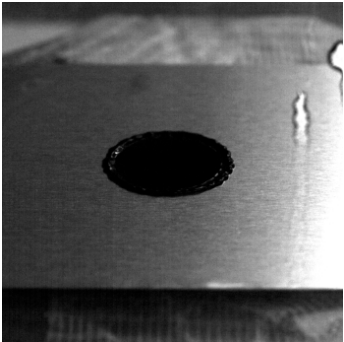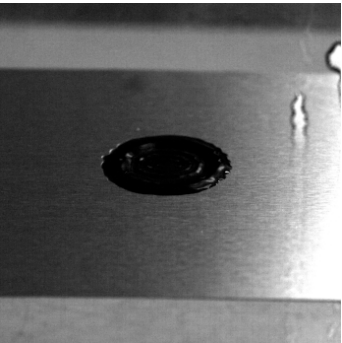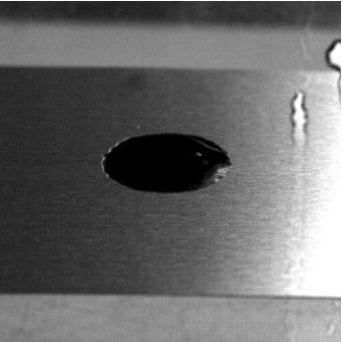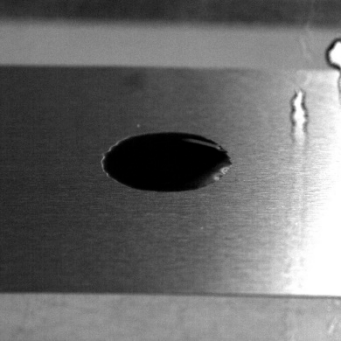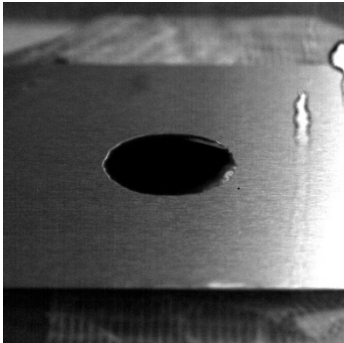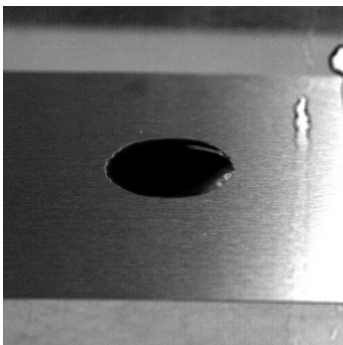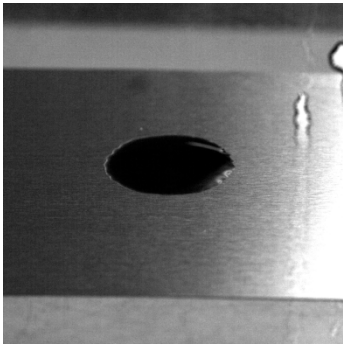
Time (ms)	(a)	(b)
6		
14		
30		
100		

Table 2. *Cont.*

Time (ms)	(a)	(b)
200		
300		
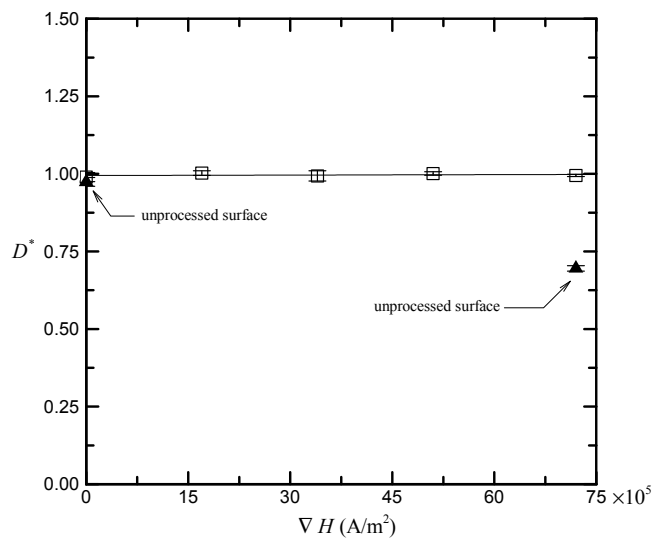
Figure 2. Reduced diameter versus magnetic field.

3.1. Effect of Surface Morphology

The comparative results of magnetic nanofluid droplet impingement on unprocessed and processed surfaces without a magnetic field are illustrated in Table 2a,c. In general, both droplets will undergo impact with the surface, spread on the surface, extend to the maximum area, then retract, and finally stop after slight vibration. The bouncing behavior does not occur on the surface for each surface. After the droplets extend to the maximum area, both droplet spreading areas seem to maintain similar values. As can be further seen in Figure 2, the processed surface exhibits a slightly higher wetted

size. This means that the degree of adhesion between the liquid and solid on the processed surface is slightly greater.

3.2. Effect of Surface Morphology with Magnetic Field

In Table 2a,b, it can be seen that a retracting behavior is displayed on the surface under an applied magnetic field gradient of 72×10^5 A/m^2 after 30 ms, causing a smaller wetted area at the final state. A lower wetted size on the unprocessed surface can also be observed in Figure 2. This may be due to the fact that the external magnetic field increases the inertial force during the retraction process and then forms a smaller wetted area on the more hydrophobic surface. However, compared with the processed surfaces, shown in Table 2c,d, the retracting behavior does not occur when the magnetic nanofluid droplet impinges on the processed surface under an applied magnetic field. Generally explaining, the nanostructures on the processed surface may further weaken the inertial force during the retraction process. This means that upon the magnetic nanofluid droplet impact on an AAO surface with a magnetic field, the AAO structure exerts a significant effect on the dynamic impact phenomenon.

3.3. Influence of Field Gradient on the Effect of Surface Morphology

To quantify the dynamic behavior of droplets impacting the processed and unprocessed surfaces at different magnetic field gradients, the normalization for the wetted size ratio has been done as D^* = the final wetted diameter/maximum extended diameter, characterizing the relative wetted size during the magnetic nanofluid droplet impact on a surface. Figure 2 shows the reduced diameter D^* versus the magnetic field gradient ∇H (from 0 to 72×10^5 A/m^2) for the case of the processed surface, so as to investigate the influence of the magnetic field gradient on the effect of surface morphology. It can be seen that the processed surface exhibits a slightly higher value of the reduced diameter D^* without an applied magnetic field, compared to the unprocessed surface (delta symbol). As mentioned in Section 3.1, the processed surface has a greater degree of adhesion between the liquid and solid. At a higher magnetic field gradient, the processed surface shows a negligible change in reduced diameter, while the unprocessed surface shows a significantly smaller reduced diameter. This means that as the magnetic field gradient increases, the surface morphology can have a more significant effect on the dynamic magnetowetting of magnetic nanofluids.

4. Conclusions

So far, no study has been conducted to investigate the dynamic behavior of magnetic nanofluid droplets on different morphological surfaces under the action of an external magnetic field. Therefore, this study has experimentally studied the dynamic characteristics of magnetic nanofluid droplet impingement on an alumina surface with/without an anodic oxidation process in an applied magnetic field. First, a water-based Fe$_3$O$_4$ nanofluid was synthesized by a co-precipitation process and stabilized using oleic acid as a surfactant. Next, an anodic oxidation treatment was performed to prepare an anodic aluminum oxide (AAO) surface with adjustable wettability, and static contact angles of magnetic nanofluid droplets on surfaces with and without anodic oxidation treatment were then obtained by a contact angle meter. Finally, the influence of surface morphology on the dynamic characteristics of magnetic nanofluid droplets impacting on the two surfaces under an applied magnetic field was investigated by using a high-speed camera. According to the results of static contact angle experiments, an aluminum sheet can be processed to obtain a more hydrophilic surface. From the dynamic images, it can be seen that the degree of adhesion between the liquid and solid on the processed surface without a magnetic field is slightly greater. If an external magnetic field is applied, the effect of AAO surface morphology will be enhanced. As a consequence, the AAO structure exerts a significant influence on the dynamic impact phenomenon of a magnetic nanofluid droplet on a solid surface with a magnetic field. This study may benefit research areas such as smart coating, spray cooling, spray painting, and jet impingement.

References

1. Yarin, A.L. Drop impact dynamics: Splashing, spreading, receding, bouncing. *Annu. Rev. Fluid Mech.* **2006**, *38*, 159–192. [CrossRef]

2. Werner, S.R.; Jones, J.R.; Paterson, A.H.; Archer, R.H.; Pearce, D.L. Droplet impact and spreading: Droplet formation effects. *Chem. Eng. Sci.* **2007**, *62*, 2336–2345. [CrossRef]

3. Liu, Y.; Li, X.L.; Yan, Y.Y.; Han, Z.W.; Ren, L.Q. Anti-icing performance of superhydrophobic aluminum alloy surface and its rebounding mechanism of droplet under super-cold conditions. *Surf. Coat. Technol.* **2017**, *331*, 7–14. [CrossRef]

4. Li, H.; Yu, S. A robust superhydrophobic surface and origins of its self-cleaning properties. *Appl. Surf. Sci.* **2017**, *420*, 336–345. [CrossRef]

5. Kim, J. Spray cooling heat transfer: The state of the art. *Int. J. Heat Fluid Flow* **2007**, *28*, 753–767. [CrossRef]

6. Ye, Q.; Domnick, J. Analysis of droplet impingement of different atomizers used in spray coating processes. *J. Coat. Technol. Res.* **2017**, *14*, 467–476. [CrossRef]

7. Xu, P.Y.; Pershin, L.; Mostaghimi, J.; Coyle, T.W. Efficient one-step fabrication of ceramic superhydrophobic coatings by solution precursor plasma spray. *Mater. Lett.* **2017**, *211*, 24–27. [CrossRef]

8. Bolleddula, D.A.; Berchielli, A.; Aliseda, A. Impact of a heterogeneous liquid droplet on a dry surface: Application to the pharmaceutical industry. *Adv. Colloid Interface Sci.* **2010**, *159*, 114–159. [CrossRef] [PubMed]

9. De Gans, B.J.; Duineveld, P.C.; Schubert, U.S. Inkjet printing of polymers: State of the art and future developments. *Adv. Mater.* **2004**, *16*, 203–213. [CrossRef]

10. Aziz, S.D.; Chandra, S. Impact, recoil and splashing of molten metal droplets. *Int. J. Heat Mass Trans.* **2000**, *43*, 2841–2857. [CrossRef]

11. Megaridis, C.M.; Boomsma, K.; Bayer, I.S. Partial rebound of molten-metal droplets impacting on solid substrates. *AIChE J.* **2004**, *50*, 1356–1363. [CrossRef]

12. Serras-Pereira, J.; Aleiferis, P.G.; Walmsley, H.L.; Davies, T.J.; Cracknell, R.F. Heat flux characteristics of spray wall impingement with ethanol, butanol, iso-octane, gasoline and E10 fuels. *Int. J. Heat Fluid Flow* **2013**, *44*, 662–683. [CrossRef]

13. Liu, Y.; Xiang, Q.; Li, Z.; Yao, S.; Liang, X.; Wang, F. Experiment and simulation investigation on the characteristics of diesel spray impingement based on droplet impact phenomenon. *Appl. Sci.* **2018**, *8*, 384. [CrossRef]

14. Worthington, A.M. On the forms assumed by drops of liquids falling vertically on a horizontal plate. *Proc. R. Soc.* **1876**, *25*, 261–272. [CrossRef]

15. Zhang, B.; Li, J.Y.; Guo, P.H.; Lv, Q. Experimental studies on the effect of Reynolds and Weber numbers on the impact forces of low-speed droplets colliding with a solid surface. *Exp. Fluids* **2017**, *58*, 125. [CrossRef]

16. Yonemoto, Y.; Kunugi, T. Analytical consideration of liquid droplet impingement on solid surfaces. *Sci. Rep.* **2017**, *7*, 2362. [CrossRef] [PubMed]

17. Sivakumar, D.; Katagiri, K.; Sato, T.; Nishiyama, H. Spreading behavior of an impacting drop on a structured rough surface. *Phys. Fluids* **2005**, *17*, 100608. [CrossRef]

18. Liu, Y.H.; Whyman, G.; Bormashenko, E.; Hao, C.L.; Wang, Z.K. Controlling drop bouncing using surfaces with gradient features. *Appl. Phys. Lett.* **2015**, *107*, 051604. [CrossRef]

19. Patil, N.D.; Bhardwaj, R.; Sharma, A. Droplet impact dynamics on micropillared hydrophobic surfaces. *Exp. Therm. Fluid Sci.* **2016**, *74*, 195–206. [CrossRef]

20. Malla, L.K.; Patil, N.D.; Bhardwaj, R.; Neild, A. Droplet Bouncing and Breakup during Impact on a Microgrooved Surface. *Langmuir* **2017**, *33*, 9620–9631. [CrossRef] [PubMed]

21. Shen, Y.; Liu, S.; Zhu, C.; Tao, J.; Chen, Z.; Tao, H.; Pan, L.; Wang, G.; Wang, T. Bouncing dynamics of impact droplets on the convex superhydrophobic surfaces. *Appl. Phys. Lett.* **2017**, *110*, 221601. [CrossRef]

22. Kwak, G.; Lee, D.W.; Kang, I.S.; Yong, K. A study on the dynamic behaviors of water droplets impacting nanostructured surfaces. *AIP Adv.* **2011**, *1*, 042139. [CrossRef]

23. Tsai, P.C.; Pacheco, S.; Pirat, C.; Lefferts, L.; Lohse, D. Drop impact upon micro- and nanostructured Superhydrophobic surfaces. *Langmuir* **2009**, *25*, 12293–12298. [CrossRef] [PubMed]

24. Raza, M.A.; Van Swigchem, J.; Jansen, H.P.; Zandvliet, H.J.W.; Poelsema, B.; Kooij, E.S. Droplet impact on hydrophobic surfaces with hierarchical roughness. *Surf. Topogr. Metrol. Prop.* **2014**, *2*, 035002. [CrossRef]

25. Taylor, R.; Coulombe, S.; Otanicar, T.; Phelan, P.; Gunawan, A.; Lv, W.; Rosengarten, G.; Prasher, R.; Tyagi, H. Small particles, big impacts: A review of the diverse applications of nanofluids. *J. Appl. Phys.* **2013**, *113*, 011301. [CrossRef]

26. Bellerová, H.; Tseng, A.A.; Pohanka, M.; Raudensky, M. Heat transfer of spray cooling using alumina/water nanofluids with full cone nozzles. *Heat Mass Transf.* **2012**, *48*, 1977–1983. [CrossRef]

27. Chang, T.B. Formation of nano-adsorption layer and its effects on nanofluid spray heat transfer performance. *J. Heat Transfer* **2015**, *137*, 021901. [CrossRef]

28. Chen, M.; He, Y.; Zhu, J.; Wen, D. Investigating the collector efficiency of silver nanofluids based direct absorption solar collectors. *Appl. Energy* **2016**, *181*, 65–74. [CrossRef]

29. Lue, Y.F.; Hung, Y.H.; Li, F.S.; Teng, T.P.; Chen, S.Y.; Wu, C.H.; Ou, Y.C. Performance assessment and scooter verification of nano-alumina engine oil. *Appl. Sci.* **2016**, *6*, 258. [CrossRef]

30. Murshed, S.M.; de Castro, C.A.N. Spreading characteristics of nanofluid droplets impacting onto a solid surface. *J. Nanosci. Nanotechnol.* **2011**, *11*, 3427–3433. [CrossRef] [PubMed]

31. Kahani, M.; Jackson, R.G.; Rosengarten, G. Experimental investigation of TiO_2/water nanofluid droplet impingement on nanostructured surfaces. *Ind. Eng. Chem. Res.* **2016**, *55*, 2230–2241. [CrossRef]

32. Rosensweig, R.E. *Ferrohydrodynamics*; Cambridge University Press: New York, NY, USA, 1985; ISBN 9780486678344.

33. Blaney, L. Magnetite (Fe_3O_4) properties, sinthesis, and applications. *Lehigh Rev.* **2007**, *15*, 32–81.

34. Mahdavi, M.; Ahmad, M.; Haron, M.; Namvar, F.; Namvar, B.; Nadi, B.; Ab Rahman, M.; Amin, J. Synthesis, surface modification and characterization of biocompatible magnetic iron oxide nanoparticles for biomedical applications. *Molecules* **2013**, *18*, 7533–7548. [CrossRef] [PubMed]

35. Latikka, M.; Backholm, M.; Timonen, J.V.I.; Ras, R.H.A. Wetting of ferrofluids: Phenomena and control. *Curr. Opin. Colloid Interface Sci.* **2018**. [CrossRef]

36. Nguyen, N.-T.; Zhu, G.; Chua, Y.-C.; Phan, V.-N.; Tan, S.-H. Magnetowetting and sliding motion of a sessile ferrofluid droplet in the presence of a permanent magnet. *Langmuir* **2010**, *26*, 12553–12559. [CrossRef] [PubMed]

37. Manukyan, S.; Schneider, M. Experimental investigation of wetting with magnetic fluids. *Langmuir* **2016**, *32*, 5135–5140. [CrossRef] [PubMed]

38. Rigoni, C.; Pierno, M.; Mistura, G.; Talbot, D.; Massart, R.; Bacri, J.-C.; Abou-Hassan, A. Static magnetowetting of ferrofluid drops. *Langmuir* **2016**, *32*, 7639–7646. [CrossRef] [PubMed]

39. Chien, Y.-C.; Weng, H.C. The effect of a magnetic field on the profile of sessile magnetic nanofluid droplets. *Smart Sci.* **2017**, *5*, 214–219. [CrossRef]

40. Chien, Y.-C.; Weng, H.C. A Brief note on the magnetowetting of magnetic nanofluids on AAO Surfaces. *Nanomaterials* **2018**, *8*, 118. [CrossRef] [PubMed]

41. Shimoiizaka, J. Flocculation and dispersion of powders in liquids. *J. Jpn. Soc. Powder Powder Metall.* **1966**, *13*, 263–274.

42. Shimoiizaka, J.; Nakatsuka, K.; Chubachi, R.; Sato, Y. On the Preparation of Magnetic Fluid and Its Behavior. *J. Jpn. Soc. Powder Powder Metall.* **1975**, *22*, 22–26. [CrossRef]

43. Shoghl, S.N.; Jamali, J.; Moraveji, M.K. Electrical conductivity, viscosity, and density of different nanofluids: An experimental study. *Exp. Therm. Fluid Sci.* **2016**, *74*, 339–346. [CrossRef]